

---

# ST-VLA: Enabling 4D-Aware Spatiotemporal Understanding for General Robot Manipulation

---

You Wu<sup>\*1</sup> Zixuan Chen<sup>\*2</sup> Cunxu Ou<sup>2</sup> Wenxuan Wang<sup>2</sup> Wenbo Huang<sup>3</sup> Lin Cao<sup>4</sup> Yangtao Chen<sup>1</sup>  
 Weichao Qiu<sup>5</sup> Xingyue Quan<sup>5</sup> Jieqi Shi<sup>2</sup> Jing Huo<sup>1</sup> Yang Gao<sup>2</sup>

## Abstract

Robotic manipulation in open-world environments requires reasoning across semantics, geometry, and long-horizon action dynamics. Existing hierarchical Vision-Language-Action (VLA) frameworks typically use 2D representations to connect high-level reasoning with low-level control, but lack depth awareness and temporal consistency, limiting robustness in complex 3D scenes. We propose **ST-VLA**, a hierarchical VLA framework using a unified 3D-4D representation to bridge perception and action. ST-VLA converts 2D guidance into 3D trajectories and generates smooth spatial masks that capture 4D spatio-temporal context, providing a stable interface between semantic reasoning and continuous control. To enable effective learning of such representations, we introduce **ST-Human**, a large-scale human manipulation dataset with 14 tasks and 300k episodes, annotated with 2D, 3D, and 4D supervision via a semi-automated pipeline. Using ST-Human, we train **ST-VLM**, a spatio-temporal vision-language model that generates spatially grounded and temporally coherent 3D representations to guide policy execution. The smooth spatial masks focus on task-relevant geometry and stabilize latent representations, enabling online replanning and long-horizon reasoning. Experiments on RL Bench and real-world manipulation tasks show that ST-VLA significantly outperforms state-of-the-art baselines, improving zero-shot success rates by 44.6% and 30.3%. These results demonstrate that offloading spatio-temporal reasoning to VLMs with

unified 3D-4D representations substantially improves robustness and generalization for open-world robotic manipulation. Project website: <https://ouc117.github.io/ST-VLA/>.

## 1. Introduction

Robust robot manipulation in open-world environments requires tightly integrating generalizable semantic understanding, accurate spatial perception, and reliable execution. Beyond identifying interaction targets, robots must reason about *how and where* to act in complex three-dimensional (3D) environments. Hierarchical Vision-Language-Action (VLA) architectures have therefore emerged as a dominant paradigm, where high-level Vision-Language Models (VLMs) perform task understanding and semantic reasoning, and low-level policies execute continuous control, improving generalization across manipulation tasks (Brohan et al., 2022; Zitkovich et al., 2023; Driess et al., 2023; Kim et al., 2024; Ahn et al., 2022; Reed et al., 2022; Chen et al., 2026).

Despite this progress, existing VLMs are primarily trained in large-scale two-dimensional (2D) images and visual question answering data, limiting their ability to model 3D geometry and long-horizon manipulation dynamics in physical environments (Radford et al., 2021; Liu et al., 2023). As a result, high-level semantic predictions often fail to align with the continuous 3D execution space required for fine-grained robotic control, leading to deviations from action, instability, and task failure (Ahn et al., 2022; Huang et al., 2023). To alleviate this issue, previous work introduces intermediate representations such as 2D waypoints, bounding boxes, or segmentation masks to connect semantic reasoning with low-level control (Liu et al., 2024; Gu et al., 2023; Ren et al., 2024; Jiang et al., 2022; Bharadhwaj et al., 2024; Yuan et al., 2024; Shridhar et al., 2022). However, these interfaces remain fundamentally constrained by the 2D paradigm. Planar representations cannot capture depth and geometric constraints, and frame-wise signals ignore temporal continuity (Ke et al., 2024; Huang et al., 2023; Chi et al., 2025; Liu et al., 2022; Goyal et al., 2023). Consequently, they lack explicit modeling of 4D (3D + time) spatio-temporal consis-

<sup>\*</sup>Equal contribution.

<sup>1</sup>School of Computer Science, Nanjing University <sup>2</sup>School of Intelligence Science and Technology, Nanjing University <sup>3</sup>School of Electronic Science and Engineering, Nanjing University <sup>4</sup>School of Instrument Science and Engineering, Southeast University <sup>5</sup>Noah’s Ark Lab, Huawei. Correspondence to: You Wu <you@smail.nju.edu.cn>.

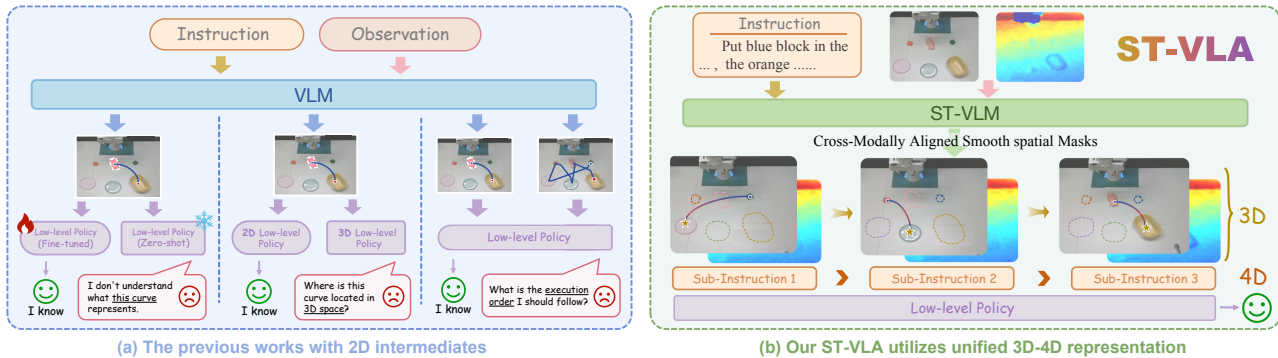


Figure 1. **ST-VLM** bridges the semantic-physical gap via unified 3D-4D spatio-temporal representations. **(Left)** Existing 2D-based VLMs face geometric ambiguity and temporal inconsistency due to the semantic-physical mismatch. **(Right)** Our **ST-VLA** utilizes unified 3D-4D representations with explicit trajectories and smooth spatial masks, ensuring robust long-horizon manipulation.

tency, often inducing action jitter and reduced robustness in dynamic or long-horizon tasks (Zheng et al., 2024).

We argue that these limitations stem from a fundamental *representation mismatch* between high-level semantic spaces and low-level physical spaces (Driess et al., 2023; Huang et al., 2023; Kerr et al., 2023; Peng et al., 2023; Jatavallabhula et al., 2023). VLM representations are rooted in static, projective visual domains, whereas robot control operates in continuous 3D physical environments. As shown in Figure 1(a), the 2D intermediates form a lossy bridge that discards critical geometric and temporal cues. This forces low-level policies to infer missing dimensions from ambiguous signals, leading to spatial misalignment and execution inaccuracy under novel viewpoints or disturbances (Huang et al., 2023; Ke et al., 2024), as well as temporal incoherence that hinders long-horizon stability (Chen et al., 2024b; 2025). An effective intermediate representation should instead jointly capture 3D geometry, temporal continuity, and cross-modal consistency.

Motivated by this insight, we propose **ST-VLA**, a hierarchical VLA framework that bridges the perception-action gap via unified 3D-4D representations. As shown in Figure 1(b), instead of rigid 2D cropping, **ST-VLA** lifts conventional 2D guidance to explicit 3D trajectories and constructs cross-modally aligned smooth spatial masks to in-paint task-irrelevant distractors. This smooth alignment ensures focus on task-relevant geometry, which preserves latent continuity, suppresses model hallucinations, and improves action stability. Moreover, by integrating 4D spatio-temporal context, **ST-VLA** enables online replanning and robust long-horizon execution. To enable high-level VLMs to produce 3D-4D representations, we introduce **ST-Human**, a large-scale dataset with 4.3M samples, built from 300K continuous human manipulation trajectories paired with high-fidelity 3D observations. Unlike prior 2D-centric or static datasets, **ST-Human** captures depth, object geometry, and temporal action evolution, providing unified spatio-

temporal supervision. Building on **ST-Human**, we propose a unified 2D-3D-4D task learning framework that extends VLM semantic reasoning across 3D spatial and 4D temporal domains. By jointly fine-tuning a 4B Qwen3-VL model (Yang et al., 2025) on **ST-Human** alongside specialized public datasets—including RoboPoint (Yuan et al., 2024), FSD (Yuan et al., 2025b), and SAT (Ray et al., 2024)—we develop **ST-VLM**. This unified training approach integrates 2D trajectory grounding, depth-aware 3D perception, and long-horizon 4D reasoning, enabling the model to acquire comprehensive spatio-temporal understanding within a single representative space. With explicit geometric and temporal constraints, **ST-VLM** learns stable, transferable 3D-4D reasoning, enabling reliable zero-shot guidance for open-world manipulation.

We evaluate **ST-VLM** and **ST-VLA** on multiple benchmark datasets as well as simulated and real-world robotic platforms. On the RoboRefit (Lu et al., 2023), CVBench (Tong et al., 2024), and SAT (Ray et al., 2024) datasets, **ST-VLM** achieves up to 33.19% improvement over existing methods. On 3 representative RL Bench tasks, **ST-VLA** improves zero-shot success rates by 44.6%. Real-world long-horizon experiments further demonstrate its execution stability and cross-scenario generalization.

Our contributions are summarized as follows: **(1)** We propose **ST-VLA**, a hierarchical Vision-Language-Action (VLA) framework built upon unified 3D-4D (3D + time) intermediate representations. **ST-VLA** replaces conventional, error-prone 2D priors with explicit 3D trajectories and latent 4D spatio-temporal context, ensuring action stability and suppressing hallucinations. **(2)** We introduce **ST-Human**, a high-fidelity 3D-4D human manipulation dataset, and propose a unified 2D-3D-4D task learning and evaluation framework. Based on this framework, we train a 4B-parameter vision-language model, **ST-VLM**, which acquires transferable 3D-4D reasoning capabilities for zero-shot open-world manipulation. **(3)** We evaluate **ST-VLM** and **ST-VLA** on

multiple benchmarks and simulated and real-world robotic platforms. Results show clear gains in zero-shot success rate, long-horizon stability, and cross-scenario generalization over existing methods.

## 2. Related Work

### 2.1. Point and Trajectory-based Spatial Guidance

An important line of research in manipulation focuses on the generalization of robotic policies by providing explicit spatial guidance. Early works utilize 2D waypoints or bounding boxes (Liu et al., 2024; Huang et al., 2024) to anchor the policy’s attention to specific image-plane coordinates. Beyond image-plane cues, another line explores 3D value-based spatial representations as guidance for manipulation (Chen et al.; Huang et al., 2023). More recently, trajectory-based task specifications emerge as a flexible interface. For example, RT-Trajectory (Gu et al., 2023) and Track2Act (Bharadhwaj et al., 2024) employ 2D gripper paths or point tracks to condition low-level execution. HAMSTER (Li et al., 2025b) further extends this paradigm hierarchically, where a VLM predicts future 2D paths to guide a conditioned 3D policy. However, these representations remain fundamentally restricted to the projective image domain, lacking the geometric fidelity and depth awareness required for precision-critical 3D manipulation. Moreover, since such signals are typically generated on a per-frame basis, they often fail to capture the temporal coherence (Zheng et al., 2024) necessary for dynamic replanning.

### 2.2. Object-Centric Grounding and Masking

To mitigate the impact of visual distractors in open-world environments, recent methods have turned to object-centric representations (Shi et al., 2024; Mirjalili et al., 2025; Hancock et al., 2025; Yuan et al., 2025a; Huang et al., 2025; Li et al., 2025a). Frameworks such as ARRO (Mirjalili et al., 2025) and PEEK (Zhang et al., 2025) leverage pre-trained segmentation models or VLM-queried points to visually isolate task-relevant objects through explicit masking. While effective at filtering clutter, existing approaches predominantly utilize hard segmentation masks like cropping in RoboPoint (Yuan et al., 2024), which, as identified in recent reasoning-driven studies (Zhao et al., 2025; Yuan et al., 2025b), can introduce discontinuities in the latent manifold. These discrete representations often lead to jittery action outputs and hallucinations due to cross-modal misalignment.

### 2.3. Vision-Language Reasoning for Manipulation

Robotic manipulation has progressed from using static vision-language representations (Parisi et al., 2022; Nair et al., 2022) to end-to-end Vision-Language-Action (VLA) models (Brohan et al., 2024; Kim et al., 2024). Although

foundation VLMs provide broad open-world semantics, their physical reasoning and generalization are often limited by weak embodied grounding (Brohan et al., 2022). To mitigate this, recent work improves spatial intelligence via supervised fine-tuning on spatial datasets (Chen et al., 2024a) or uses reinforcement learning to elicit stronger reasoning (Guo et al., 2025; Yuan et al., 2025d). A key bottleneck is the lack of high-quality continuous 3D/4D data linking semantic intent to execution. Existing VLA systems largely rely on large-scale robot demonstrations (Walke et al., 2023; Khazatsky et al., 2024), which are costly to scale, or simulation-to-real transfer (James et al., 2020; Tao et al., 2024), which remains hindered by domain gaps. In contrast, we propose ST-Human, a high-fidelity human manipulation dataset with dense 3D/4D annotations that capture continuous execution flows, enabling ST-VLM to learn anchor-based depth estimation and long-horizon reasoning.

## 3. Methodology

### 3.1. Problem Formulation

We consider the problem of an embodied agent executing manipulation tasks in open-world environments guided by a natural language instruction  $l \in \mathcal{L}$ . At each timestep  $t$ , the agent receives a single-view RGB-D observation  $\mathbf{o}_t \in \mathcal{O}$  and a robot state  $\mathbf{s}_t \in \mathcal{S}$ . Following the established paradigm of 3D-aware policies, the raw observation  $\mathbf{o}_t$  is unprojected into a 3D point cloud  $\mathbf{P}_t$  in the robot’s base frame. The objective is to learn a mapping that generates a sequence of actionable keyposes  $\mathbf{a}_t \in SE(3)$ , which are subsequently translated by a deterministic motion planner into continuous joint control commands.

### 3.2. Hierarchical VLA Architecture Overview

To bridge semantic reasoning with physical execution, we decouple the manipulation policy into a hierarchy: a high-level vision-language model  $\pi_{hi}$  and a low-level execution policy  $\pi_{lo}$ . The high-level  $\pi_{hi}$  is derived from a pre-trained general-purpose VLM and is specialized through supervised fine-tuning on large-scale datasets encompassing diverse robotic manipulation tasks. This specialization enables the VLM to function as a spatio-temporal reasoner. Given the observation  $\mathbf{o}_t$  and instruction  $l$ ,  $\pi_{hi}$  generates a unified intermediate representation  $\mathcal{Z}$  and, in long-horizon scenarios, produces an updated sub-instruction  $l'$  to guide subsequent execution. This process is formulated as:

$$(\mathcal{Z}, l') = \pi_{hi}(\mathbf{o}_t, l), \quad (1)$$

where  $\mathcal{Z} = \{\tau, \mathcal{M}\}$  consists of a 3D trajectory  $\tau$  and a corresponding spatial mask  $\mathcal{M}$ . In short-horizon tasks where the initial instruction is sufficient, the instruction remains invariant such that  $l' = l$ .

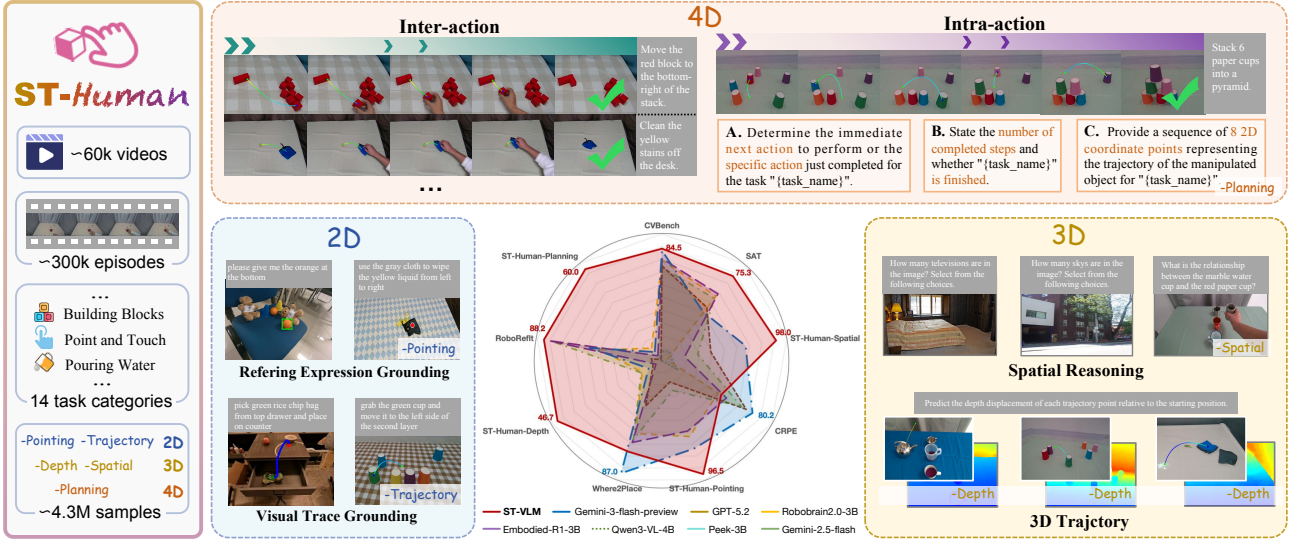


Figure 2. Overview of the ST-Human Dataset Construction and Unified 2D-3D-4D Task Generation.

The low-level policy  $\pi_{lo}$  is responsible for control within an augmented observation space. We define an augmentation function  $\psi$  that integrates the spatio-temporal guidance  $\mathcal{Z}$  into the observation stream  $\tilde{\mathbf{o}}_t = \psi(\mathbf{o}_t, \mathcal{Z})$ . This allows  $\pi_{lo}$  to use the spatial priors from  $\pi_{hi}$  without architectural changes. The spatial masks in  $\mathcal{M}$  are implemented with smooth boundaries for stable feature extraction. Finally,  $\pi_{lo}$  maps the augmented observation, the robot state, and the potentially updated instruction to the target keypose  $\mathbf{a}_t$ :

$$\mathbf{a}_t = \pi_{lo}(\tilde{\mathbf{o}}_t, \mathbf{s}_t, l^t). \quad (2)$$

By offloading semantic reasoning and spatial grounding to  $\pi_{hi}$ , our framework enables  $\pi_{lo}$  to focus on geometric execution and enhance zero-shot generalization.

### 3.3. Spatio-Temporal VLM Learning with ST-Human

To support the hierarchical architecture in Sec. 3.2, we introduce **ST-Human**, a high-fidelity dataset that provides the supervision needed for a general-purpose VLM  $\pi_{hi}$  to learn spatial and temporal reasoning. This section describes large-scale data collection and the generation of 2D, 3D, and 4D supervisory tasks.

#### 3.3.1. SCALABLE 3D-4D DATASET CONSTRUCTION

We record  $\sim 60k$  videos (300k episodes) across 14 single-arm tabletop manipulation categories using a fixed RGB-D sensor; see Appendix C. To ground the pipeline in physical constraints, we annotate initial/final 2D contact points, object semantics, and relative spatial configurations for a core subset, and develop an annotation interface (Appendix A). These labels serve as deterministic seeds for automated annotation at scale, reducing error accumulation compared to

purely heuristic methods.

Following collection, a fully automated pipeline organizes supervision into 2D, 3D, and 4D task groups for multi-task fine-tuning (Figure 2). **2D spatial tasks** target image-plane grounding and tracking. We back-project the annotated 3D grasp points to pixel coordinates for semantic-to-pixel alignment and utilize SAM2 with video tracking to generate 2D keypoint trajectories. **3D geometric tasks** incorporate depth and relational structure. We synthesize 3D trajectories by fusing 2D motion flows with aligned depth maps and lifting waypoints into workspace coordinates. A relational module converts spatial labels into dense supervision over relative object positions and orientations, forming a scene-graph style representation. Finally, **4D spatio-temporal tasks** model action evolution over time. By linking dependent episodes within the same video, we train  $\pi_{hi}$  to reason about task progress and plan across actions. Within each episode,  $\pi_{hi}$  predict the remaining trajectory from partial observations, encouraging dynamic replanning and maintaining representation coherence during execution. See Appendix B for details.

#### 3.3.2. UNIFIED VLM FINE-TUNING AND SPATIO-TEMPORAL INFERENCE

To equip  $\pi_{hi}$  with specialized 3D-4D reasoning, we implement a two-stage supervised fine-tuning (SFT) strategy and a hierarchical inference protocol that lifts 2D visual cues to 3D execution space (see Figure 3).

During training, we first leverage public multimodal datasets for general semantic reasoning, followed by domain-specific SFT on ST-Human. The prompts used for fine-tuning are provided in Appendix F. The model learns to map instruc-

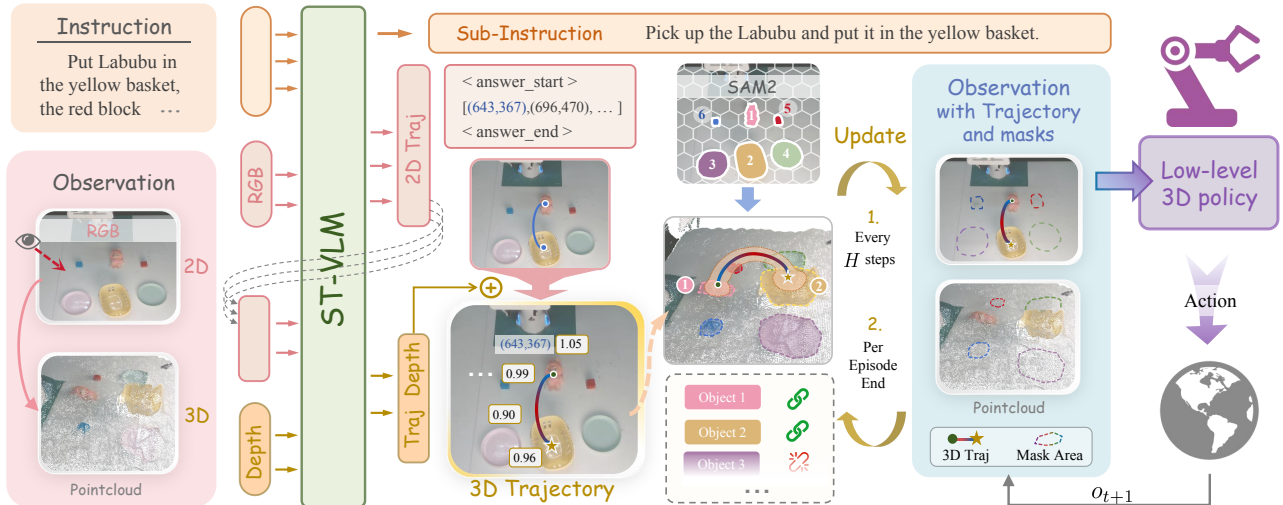


Figure 3. **The ST-VLA Pipeline.** Given a global instruction and an RGB-D observation, the high-level **ST-VLM** generates sub-instructions and 2D trajectories. These are lifted to 3D and fused with SAM2 masks to form a unified 3D-4D representation, which conditions the low-level 3D policy for continuous action execution. Guidance is refreshed every  $H$  steps for replanning and robustness to disturbances.

Table 1. **VLM Performance Comparison on Selected 2D, 3D, and 4D Benchmarks.** Best results are bolded.

Method	2D Tasks				3D Tasks				4D Tasks
	RoboRefit	Where2Place	ST-Human-Pointing	CVBench	SAT	CRPE	ST-Human-Spatial	ST-Human-Depth	ST-Human-Planning
<i>Closed-source models</i>									
GPT-5.2	16.65%	43.00%	20.50%	79.62%	66.00%	78.89%	68.00%	4.00%	88.00%
Gemini-3-flash	57.75%	<b>87.00%</b>	75.50%	83.94%	64.67%	<b>80.21%</b>	84.00%	6.00%	84.00%
<i>Open-source models</i>									
PEEK-3B	10.05%	14.00%	3.00%	55.49%	52.67%	64.55%	50.00%	0.00%	88.00%
Qwen3VL-4B	83.63%	65.00%	27.50%	79.21%	68.67%	77.89%	62.00%	9.33%	88.00%
Robobrain2.0-3B	50.61%	61.00%	65.50%	81.22%	69.33%	73.03%	48.00%	8.89%	88.00%
Embodied-R1-3B	85.05%	66.83%	61.00%	81.69%	70.00%	74.78%	56.00%	2.70%	78.00%
<b>ST-VLA (Ours)</b>	<b>88.15%</b>	73.00%	<b>96.50%</b>	<b>84.52%</b>	<b>75.33%</b>	73.67%	<b>98.00%</b>	<b>46.67%</b>	<b>92.00%</b>

tions and observations to structured text outputs, including normalized 2D coordinates  $\mathbf{x} \in [0, 1]^2$ . Building on these representations, we resolve the geometric ambiguity that a planar trajectory  $\tau_{2D}$  may map to multiple 3D paths. Given an RGB image and a colorized depth map,  $\pi_{hi}$  predicts  $\tau_{2D}$  and retrieves the ground-truth starting depth  $d_{start}$  from the depth input. It then predicts relative depth offsets for subsequent waypoints. These offsets represent intended end-effector depth rather than static surface depth.

During deployment, the VLM runs every  $H$  timesteps, balancing compute efficiency with stable long-horizon planning. Each update follows two stages. First, the VLM predicts a projected 2D trajectory  $\tau_{2D}$  from the target object to the goal given the current RGB observation and instruction  $l$ . Second, it lifts  $\tau_{2D}$  to 3D  $\tau_{3D}$  by combining RGB-D observations with the anchored starting depth  $d_{start}$  and predicting relative depth offsets along the waypoints. The resulting  $\tau_{3D}$  provides a continuous spatial condition for the low-level policy  $\pi_{lo}$  until the next update.

### 3.4. Hierarchical 3D Control via Unified Representation

To bridge reasoning and execution, we define a unified intermediate representation  $\mathcal{Z}$  that combines spatial-temporal paths and geometric constraints into a single guidance signal. This section describes how  $\mathcal{Z}$  is generated and how it is injected cross-modally to condition the low-level policy.

#### 3.4.1. SPATIO-TEMPORAL GUIDANCE CONSTRUCTION

In long-horizon scenarios, the high-level model  $\pi_{hi}$  first decomposes the initial global instruction  $l$  into atomic, action-specific sub-instructions  $l'$ , whereas  $l'$  and  $l$  are equivalent in short-term tasks. Guided by the refined instruction,  $\pi_{hi}$  predicts the 3D trajectory  $\tau_{3D} = \{\mathbf{p}_1, \dots, \mathbf{p}_K\}$ , which is later expanded into a spatial tube  $\mathcal{T}$ . This tube is defined by a cylindrical expansion with a fixed radius  $r$ , such that  $\mathcal{T} = \bigcup_{k=1}^K \mathcal{B}(\mathbf{p}_k, r)$ , where  $\mathcal{B}(\mathbf{p}, r)$  denotes a 3D ball centered at  $\mathbf{p}$ .  $\mathcal{T}$  highlights the safe and intended operational volume for the robot’s end-effector.

We introduce a selective masking mechanism to isolate task-

Table 2. Results on Simulated Robot Manipulation Tasks. Background colors highlight ST-VLA variants.

	Method	Close Jar		Light Bulb In		Put Groceries		Average	
		Seen	Unseen	Seen	Unseen	Seen	Unseen	Seen	Unseen
Single-task	3DDA (Baseline)	71.9 $\pm$ 3.0	44.4 $\pm$ 9.6	20.8 $\pm$ 3.6	25.9 $\pm$ 6.4	33.3 $\pm$ 3.0	00.0 $\pm$ 0.0	42.0	23.4
	ST-VLA w/ 3DDA (Frozen)	98.2 $\pm$ 3.0	66.7 $\pm$ 0.0	37.5 $\pm$ 0.0	25.9 $\pm$ 17.0	42.1 $\pm$ 5.3	5.6 $\pm$ 9.6	59.3	32.7
	<b>ST-VLA w/ 3DDA (FT)</b>	<b>100.0<math>\pm</math>0.0</b>	<b>100.0<math>\pm</math>0.0</b>	<b>45.8<math>\pm</math>3.6</b>	<b>81.5<math>\pm</math>6.4</b>	<b>54.4<math>\pm</math>8.0</b>	<b>16.7<math>\pm</math>16.7</b>	<b>66.7</b>	<b>66</b>
	3DFA (Baseline)	61.4 $\pm$ 3.0	38.9 $\pm$ 9.6	22.9 $\pm$ 3.6	11.1 $\pm$ 0.0	5.3 $\pm$ 5.3	00.0 $\pm$ 0.0	29.9	16.7
	ST-VLA w/ 3DFA (Frozen)	68.4 $\pm$ 5.3	44.4 $\pm$ 9.6	<b>41.7<math>\pm</math>3.6</b>	11.1 $\pm$ 0.0	12.3 $\pm$ 3.0	00.0 $\pm$ 0.0	40.8	18.5
	<b>ST-VLA w/ 3DFA (FT)</b>	<b>91.2<math>\pm</math>6.1</b>	<b>72.2<math>\pm</math>9.6</b>	39.6 $\pm$ 7.2	<b>59.3<math>\pm</math>6.4</b>	<b>56.1<math>\pm</math>8.0</b>	<b>11.1<math>\pm</math>9.6</b>	<b>62.3</b>	<b>47.5</b>
Multi-task	3DDA (Baseline)	75.4 $\pm$ 3.0	11.1 $\pm$ 9.6	56.3 $\pm$ 0.0	37.0 $\pm$ 12.8	63.2 $\pm$ 5.3	00.0 $\pm$ 0.0	65.0	16.0
	ST-VLA w/ 3DDA (Frozen)	<b>100.0<math>\pm</math>0.0</b>	55.6 $\pm$ 9.6	<b>68.8<math>\pm</math>6.3</b>	59.3 $\pm$ 6.4	54.4 $\pm$ 3.0	00.0 $\pm$ 0.0	74.4	38.3
	<b>ST-VLA w/ 3DDA (FT)</b>	<b>98.2<math>\pm</math>3.0</b>	<b>100.0<math>\pm</math>0.0</b>	54.2 $\pm$ 3.6	<b>81.5<math>\pm</math>6.4</b>	<b>73.7<math>\pm</math>0.0</b>	<b>22.2<math>\pm</math>9.6</b>	<b>75.4</b>	<b>67.9</b>
	3DFA (Baseline)	71.9 $\pm$ 3.0	44.4 $\pm$ 9.6	<b>66.7<math>\pm</math>7.2</b>	00.0 $\pm$ 0.0	49.1 $\pm$ 3.0	5.6 $\pm$ 9.6	62.6	16.7
	ST-VLA w/ 3DFA (Frozen)	93.3 $\pm$ 3.0	67.7 $\pm$ 16.7	64.6 $\pm$ 3.6	29.6 $\pm$ 6.4	56.1 $\pm$ 11.0	11.1 $\pm$ 9.6	<b>71.3</b>	36.1
	<b>ST-VLA w/ 3DFA (FT)</b>	<b>98.2<math>\pm</math>3.0</b>	<b>100.0<math>\pm</math>0.0</b>	54.2 $\pm$ 3.6	<b>81.5<math>\pm</math>6.4</b>	<b>56.1<math>\pm</math>3.0</b>	<b>27.8<math>\pm</math>9.6</b>	69.5	<b>69.7</b>

Table 3. Success rates on long-horizon *push-button* tasks across three seeds, evaluated ST-VLA(3DFA) on seen buttons and unseen multi-step sequences.

Category	Success Rate (%)
Seen Tasks	97.4 $\pm$ 4.4
LH 2-step (Unseen)	93.3 $\pm$ 11.5
LH 3-step (Unseen)	100.0 $\pm$ 0.0
<b>Overall</b>	<b>97.3<math>\pm</math>2.3</b>

relevant geometry. First, we unproject SAM2-generated dense instance segmentation  $\{M_i\}$  into the 3D workspace. An object is identified as task-relevant if its occupancy  $\mathcal{V}_i$  intersects with the spatial tube, i.e.,  $\mathcal{V}_i \cap \mathcal{T} \neq \emptyset$ . For all task-irrelevant objects, we apply a cross-modal smoothing operator to both RGB and depth channels. Non-relevant mask regions are inpainted via interpolation, constrained by RGB color gradients and neighboring depth values to preserve local feature coherence. This approach ensures cross-modal alignment and prevents instability in the policy’s latent manifold.

The final augmented observation  $\tilde{\mathbf{o}}_t$  overlays the 2D projection of  $\tau_{3D}$  on the inpainted RGB image with a translucent red-to-blue gradient to encode depth. Together with the refined instruction  $l'$ , it is fed to the low-level policy  $\pi_{l_0}$ , focusing attention on the task-relevant spatial manifold.

### 3.4.2. 3D-AWARE POLICY SPECIALIZATION

We adopt 3D Diffuser Actor (3DDA) (Ke et al., 2024) and 3D FlowMatch Actor (3DFA) (Gkanatsios et al., 2025) as low-level backbones for their robust 3D-aware representations from single-view RGB-D input. 3DDA models action distributions via denoising, while 3DFA regresses trajectory segments through flow matching. Both map the unprojected point cloud  $\mathbf{P}_t$  to accurate  $SE(3)$  keyposes for execution by a motion planner. We specialize these models via imitation learning on augmented expert demonstrations. Rather than using dense trajectory policies, we adopt keypose-based training, extracting sequential keypose coordinates to reconstruct the ground-truth 3D guidance.

During training, we apply the same augmentation function  $\psi$  (Sec. 3.4.1) to the raw observations. Concretely, we render the ground-truth trajectory onto the RGB image and apply cross-modal smooth spatial masks to the RGB-D input. This strategy encourages the policy  $\pi_{l_0}$  to align its attention with the VLM-provided spatio-temporal priors. At inference time  $\pi_{l_0}$  can reliably track the operation tube while suppressing distractors outside the masked regions.

A key advantage of our smooth masking is its robustness to observation shifts. Unlike traditional brittle binary truncation, smooth boundary transitions preserve feature continuity and manifold stability. This design further allows our framework to function with vanilla policies trained on raw, unaugmented data. In such frozen-policy configurations, where the low-level policy  $\pi_{l_0}$  is used without task-specific retraining on augmented data. The smooth mask acts as a high-level attention filter that concentrates the policy’s focus on task-relevant geometries. We omit the explicit trajectory visualization to avoid confusing the frozen policy, retaining only the spatial masking.

## 4. Experiments

### 4.1. Evaluation of ST-VLM Capabilities

We evaluate our model on nine benchmarks across 2D, 3D, and 4D dimensions (Table 1). This suite includes established open-source datasets (RoboRefit (Lu et al., 2023), Where2Place (Yuan et al., 2024), CVBench (Tong et al., 2024), SAT (Ray et al., 2024), and CRPE (Wang et al., 2024)) and our proprietary ST-Human series, which comprises ST-Human-Pointing (Point Detection), -Trajectory (Predicting 2D trajectory), -Spatial (Spatial Understanding), -Depth (Trajectory Depth Estimation), and -Planning (4D Temporal Reasoning).

We compare our model against six state-of-the-art (SOTA) baselines, consisting of four specialized open-source models: Embodied-R1-3B (Yuan et al., 2025c), PEEK-3B (Zhang et al., 2025), Robobrain2.0-3B (Team et al.,

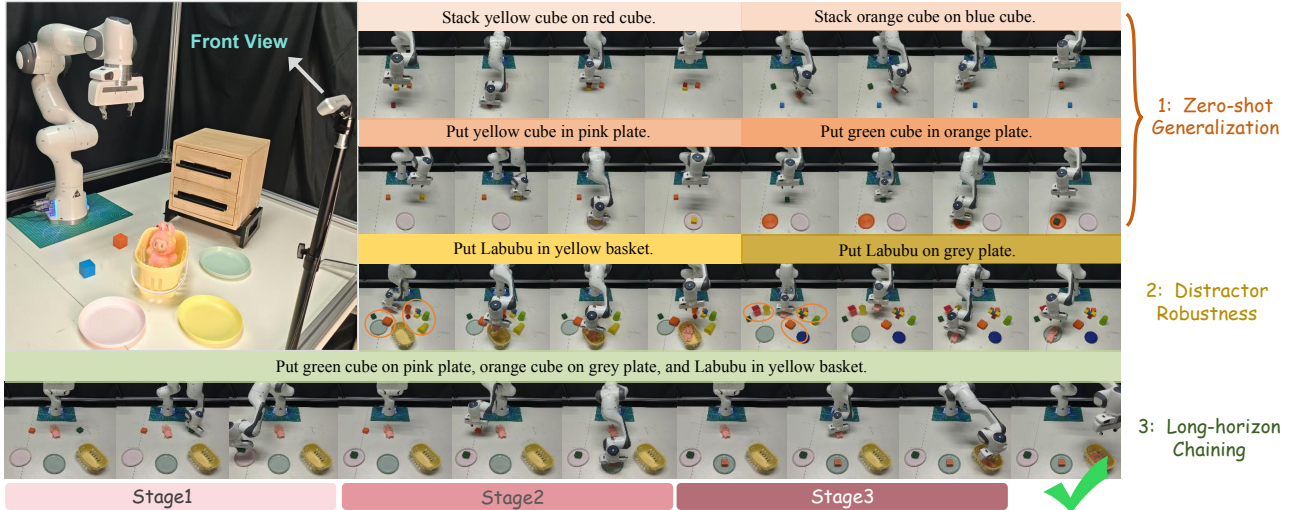


Figure 4. Real-world experimental evaluation of ST-VLA. Left: Franka Emika Panda hardware setup. Right: Qualitative results across three dimensions: (1) zero-shot generalization to unseen object categories and geometries; (2) distractor robustness under task-irrelevant visual clutter; and (3) long-horizon chaining via sequential execution of multiple placement tasks.

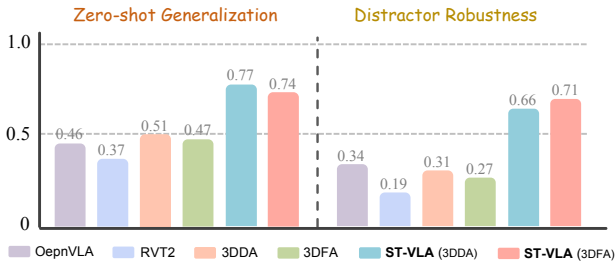


Figure 5. Real-world zero-shot generalization results.

2025), and our base model Qwen3VL-4B (Yang et al., 2025); and two leading closed-source models: GPT-5.2 (OpenAI, 2025) and Gemini-3-pro-preview (DeepMind, 2025). All evaluations are conducted across both existing open-source benchmarks and our curated ST-Human dataset to assess zero-shot generalization and task-specific precision. Detailed hyperparameters are provided in Table 7. More experimental results on VLM capabilities and metric definitions are provided in Appendix I.

The comparative results are summarized in Table 1. Overall, our model achieves competitive performance across all categories. Several key observations emerge from the data:

1) *Superior Spatio-Temporal Precision*: ST-VLA demonstrates a significant lead in ST-Human-Depth and 4D Tasks. It achieves 46.67% accuracy in depth estimation, far surpassing the best baseline (9.33%), and maintains temporal coherence in long-horizon planning (92.00% vs. 88.00%). This performance gain is attributed to the high-fidelity annotations in ST-Human, which empower the VLM to transition from static 2D grounding to dynamic 3D-aware reasoning.

2) *Robustness in 3D Understanding*: While closed-source models like GPT-5.2 show strong semantic reasoning (e.g., on CVBench), they often struggle with precise spatial grounding in robotic workspaces. ST-VLA outperforms these general-purpose VLMs on ST-Human-Spatial (98.00% vs. 84.00%) and ST-Human-Pointing (96.50% vs. 75.50%), indicating that specialized fine-tuning on embodied data is essential for manipulation-level precision.

3) *Efficiency and Generalization*: Despite having fewer parameters than largest closed-source counterparts like Gemini-3-flash, our 4B-parameter ST-VLA exhibits superior transferability on unseen ST-Human-Planning tasks. With a 92.00% success rate, it effectively estimates current task progress and predicts previous and next steps, indicating that that compact, domain-specific models can outperform general-purpose giants in complex temporal reasoning.

The evaluation validates that our fine-tuned ST-VLM successfully functions as a robust high-level reasoner within the hierarchical framework. By effectively distilling 3D spatial priors and 4D temporal context, the model provides a solid foundation for the subsequent low-level execution policy to master complex, long-horizon tasks in the open world.

## 4.2. Evaluation of ST-VLA Capabilities

### 4.2.1. SIMULATION EXPERIMENTS

**Simulation Tasks.** To evaluate ST-VLA in open-world manipulation, we conduct extensive simulation experiments on RL Bench (James et al., 2020) with four representative tasks. We use three tasks—*Close Jar*, *Light Bulb In*, and *Put Groceries In Cupboard*—to test generalization across

variations in object color, pose, and geometry. We further include the long-horizon *Push Buttons* task to assess temporal reasoning and task decomposition. To assess robustness against out-of-distribution (OOD) scenarios, we partition the dataset into **Seen** and **Unseen** subsets based on variations (see Appendix D for details). The Unseen subset contains novel colors and object shapes absent from training, posing a significant challenge to standard imitation learning. We consider two settings: **Single-task**, where a task-specific lower-level policy is trained and tested per task; and **Multi-task**, where a unified lower-level policy is trained across all four tasks to handle diverse manipulation goals.

**Baselines.** We report results for two ST-VLA variants: (1) **ST-VLA w/ Frozen Policy**, which uses a base policy without specialized retraining and receives VLM guidance only during inference; and (2) **ST-VLA w/ Fine-tuned (FT) Policy**, where the low-level model is trained from scratch on data processed using VLM-provided intermediate representations. All results are averaged over three random seeds. We use 3DDA (Ke et al., 2024) and 3DFA (Gkanatsios et al., 2025) as the low-level policies, and also include them as baselines to demonstrate that our proposed 3D-4D intermediate representations improve low-level policy generalization. Detailed hyperparameters are provided in Table 8.

**Analysis of Simulation Results.** As shown in Table 2, ST-VLA consistently improves success rates for both 3DDA and 3DFA, demonstrating broad applicability. The largest gains appear in Unseen scenarios, where vanilla imitation learning models often fail under distribution shift, with our fine-tuned (FT) version improving zero-shot success rates by **44.6%**. ST-VLA equips robots with robust semantic and spatial priors. Even in Seen tasks, ST-VLA outperforms the baselines by simplifying the execution space. By masking task-irrelevant distractors, ST-VLA isolates the relevant spatial manifold and reduces the perceptual complexity, allowing  $\pi_{lo}$  to focus exclusively on geometric execution.

Notably, the Frozen variant achieves substantial gains without specialized retraining. This validates that our smooth masks effectively focus attention while maintaining latent manifold stability. Unlike previous hierarchical methods that require joint fine-tuning, ST-VLA seamlessly integrates with existing imitation learning algorithms.

To further assess temporal reasoning, we decompose the *Push Buttons* task into short-horizon primitives. Although the low-level policy  $\pi_{lo}$  (trained with 3DFA) sees only single-button press episodes during training, it achieves a **93.3% success rate** on the original long-horizon test set (sequentially pressing 2-3 buttons) when guided by ST-VLA (as shown in Table 3). This demonstrates that our framework effectively delegates task decomposition and sequence planning to the high-level VLM. By offloading temporal complexity, the low-level policy no longer needs to learn

long-horizon trajectories, yet can execute complex multi-step sequences through modular, primitive-based control.

Finally, the full ST-VLA (FT) version exceeds the success rates of baseline models even when the latter are trained on the complete dataset. This indicates that hierarchical decomposition not only facilitates zero-shot transfer but also fundamentally raises the performance ceiling of low-level controllers in complex, multi-object environments.

#### 4.2.2. REAL-WORLD EXPERIMENTS

To validate real-world applicability and zero-shot generalization of ST-VLA, we conduct physical experiments using a Franka Emika Panda robot arm. We focus on objects-placing and block-stacking tasks evaluate semantic-to-spatial grounding (Figure 4). For seen scenarios, we collect a limited set of demonstration trajectories per task to train the low-level policy. Details of the real-world experimental setup and task definitions are provided in Appendix G. To rigorously assess the model’s robustness, we introduce three evaluation dimensions: (1) **Zero-shot Generalization**, featuring unseen object categories and geometries; (2) **Distractor Robustness**, introducing task-irrelevant objects to clutter the workspace; and (3) **Long-horizon Chaining**, sequentially executing three consecutive manipulation stages. For the first two dimensions, we evaluate 7 distinct experimental settings with 10 trials each to provide a statistically robust performance analysis.

As illustrated in Fig. 5, ST-VLA significantly outperforms baseline 3D policies, yielding average success rate improvements of **30.3%** in zero-shot generalization and **40.8%** in distractor robustness. For OOD objects, ST-VLM leverages semantic knowledge to synthesize 3D guidance, compensating for the low-level policy’s limited exposure. In cluttered scenes, our smooth masking suppresses task-irrelevant features, stabilizing the latent manifold and preventing the visual-noise-induced failures common in imitation learning.

In addition, ST-VLA effectively handles long-horizon tasks, achieving over 70% success rate throughout triple-placement sequences despite being trained on short-horizon, single-action demonstrations. By offloading temporal reasoning and sub-goal planning tasks to the VLM, the framework decomposes complex multi-stage instructions into executable 3D-guided primitives. The consistent real-world performance confirms that decoupling semantic-temporal reasoning from execution via a 3D-aware interface allows robots to perform sophisticated manipulation with minimal human demonstrations.

## 5. Conclusion and Discussion

We presented ST-VLA, a hierarchical framework bridging the perception-action gap in open-world robotic manipula-

tion. By introducing a unified 3D-4D representation comprising 3D trajectories and cross-modally aligned smooth spatial masks, we decouple high-level semantic reasoning from low-level geometric execution. This architecture leverages latent 4D spatio-temporal context to enable both intra-action replanning and inter-action long-horizon planning.

To support this, we introduced ST-Human, a large-scale human manipulation dataset with high-fidelity 3D-4D annotations for specialized VLM fine-tuning. Experimentals in RL-Bench and real-world scenarios demonstrate that ST-VLA achieves superior zero-shot generalization, significantly outperforming state-of-the-art baselines on unseen tasks and cluttered environments. By offloading spatiotemporal complexity to a specialized VLM, ST-VLA provides a robust and scalable pathway toward general-purpose robot manipulation in the open world.

**Limitations and Future Work.** While ST-VLA shows robust generalization, its performance may degrade in extreme clutter where SAM2 struggles with ambiguous segmentation. Additionally, our current interface is primarily optimized for single-view execution. Future work will focus on integrating more resilient multi-view perception and adapting our hierarchical guidance to a broader range of low-level backbones, aiming to establish a truly universal and versatile framework for open-world manipulation.

## References

- Ahn, M., Brohan, A., Brown, N., Chebotar, Y., Cortes, O., David, B., Finn, C., Fu, C., Gopalakrishnan, K., Hausman, K., et al. Do as i can, not as i say: Grounding language in robotic affordances. *arXiv preprint arXiv:2204.01691*, 2022.
- Bharadhwaj, H., Mottaghi, R., Gupta, A., and Tulsiani, S. Track2act: Predicting point tracks from internet videos enables generalizable robot manipulation. In *European Conference on Computer Vision*, pp. 306–324, 2024.
- Brohan, A., Brown, N., Carbajal, J., Chebotar, Y., Dabis, J., Finn, C., Gopalakrishnan, K., Hausman, K., Herzog, A., Hsu, J., et al. Rt-1: Robotics transformer for real-world control at scale. *arXiv preprint arXiv:2212.06817*, 2022.
- Brohan, A., Brown, N., Carbajal, J., Chebotar, Y., Chen, X., Choromanski, K., Ding, T., Driess, D., Dubey, A., Finn, C., et al. Rt-2: Vision-language-action models transfer web knowledge to robotic control, 2023. *URL* <https://arxiv.org/abs/2307.15818>, 2024.
- Chen, B., Xu, Z., Kirmani, S., Ichter, B., Sadigh, D., Guibas, L., and Xia, F. Spatialvlm: Endowing vision-language models with spatial reasoning capabilities. In *Proceedings of the IEEE/CVF Conference on Computer Vision and Pattern Recognition*, pp. 14455–14465, 2024a.
- Chen, Y., Chen, Z., Yin, J., Huo, J., Tian, P., Shi, J., and Gao, Y. Gravmad: Grounded spatial value maps guided action diffusion for generalized 3d manipulation. In *The Thirteenth International Conference on Learning Representations*.
- Chen, Z., Ji, Z., Huo, J., and Gao, Y. Scar: Refining skill chaining for long-horizon robotic manipulation via dual regularization. *Advances in Neural Information Processing Systems*, 37:111679–111714, 2024b.
- Chen, Z., Huo, J., Chen, Y., and Gao, Y. Robohorizon: An llm-assisted multi-view world model for long-horizon robotic manipulation. *arXiv preprint arXiv:2501.06605*, 2025.
- Chen, Z., Yin, J., Chen, Y., Huo, J., Tian, P., Shi, J., Hou, Y., Li, Y., and Gao, Y. Deco: Task decomposition and skill composition for zero-shot generalization in long-horizon 3d manipulation. *IEEE Robotics and Automation Letters*, 2026.
- Chi, C., Xu, Z., Feng, S., Cousineau, E., Du, Y., Burchfiel, B., Tedrake, R., and Song, S. Diffusion policy: Visuomotor policy learning via action diffusion. *The International Journal of Robotics Research*, 44(10-11): 1684–1704, 2025.
- DeepMind, G. Gemini-3-pro-preview: Model card and preview release. <https://deepmind.google/models/gemini/pro/>, 2025. accessed 2026-01-29.
- Driess, D., Xia, F., Sajjadi, M. S., Lynch, C., Chowdhery, A., Wahid, A., Tompson, J., Vuong, Q., Yu, T., Huang, W., et al. Palm-e: An embodied multimodal language model. 2023.
- Gkanatsios, N., Xu, J., Bronars, M., Mousavian, A., Ke, T.-W., and Fragkiadaki, K. 3d flowmatch actor: Unified 3d policy for single-and dual-arm manipulation. *arXiv preprint arXiv:2508.11002*, 2025.
- Goyal, A., Xu, J., Guo, Y., Blukis, V., Chao, Y.-W., and Fox, D. Rvt: Robotic view transformer for 3d object manipulation. In *Conference on Robot Learning*, pp. 694–710. PMLR, 2023.
- Gu, J., Kirmani, S., Wohlhart, P., Lu, Y., Arenas, M. G., Rao, K., Yu, W., Fu, C., Gopalakrishnan, K., Xu, Z., et al. Rt-trajectory: Robotic task generalization via hindsight trajectory sketches. *arXiv preprint arXiv:2311.01977*, 2023.
- Guo, D., Yang, D., Zhang, H., Song, J., Zhang, R., Xu, R., Zhu, Q., Ma, S., Wang, P., Bi, X., et al. Deepseek-r1: Incentivizing reasoning capability in llms via reinforcement learning. *arXiv preprint arXiv:2501.12948*, 2025.

- Hancock, A. J., Ren, A. Z., and Majumdar, A. Run-time observation interventions make vision-language-action models more visually robust. In *2025 IEEE International Conference on Robotics and Automation (ICRA)*, pp. 9499–9506. IEEE, 2025.
- Huang, H., Liu, F., Fu, L., Wu, T., Mukadam, M., Malik, J., Goldberg, K., and Abbeel, P. Otter: A vision-language-action model with text-aware visual feature extraction. *arXiv preprint arXiv:2503.03734*, 2025.
- Huang, S., Ponomarenko, I., Jiang, Z., Li, X., Hu, X., Gao, P., Li, H., and Dong, H. Manipvqa: Injecting robotic affordance and physically grounded information into multimodal large language models. In *2024 IEEE/RSJ International Conference on Intelligent Robots and Systems (IROS)*, pp. 7580–7587. IEEE, 2024.
- Huang, W., Wang, C., Zhang, R., Li, Y., Wu, J., and Fei-Fei, L. Voxposer: Composable 3d value maps for robotic manipulation with language models. In *Conference on Robot Learning*, pp. 540–562. PMLR, 2023.
- James, S., Ma, Z., Arrojo, D. R., and Davison, A. J. Rlbench: The robot learning benchmark & learning environment. *IEEE Robotics and Automation Letters*, 5(2):3019–3026, 2020.
- Jatavallabhula, K. M., Kuwajerwala, A., Gu, Q., Omama, M., Chen, T., Maalouf, A., Li, S., Iyer, G., Saryazdi, S., Keetha, N., et al. Conceptfusion: Open-set multimodal 3d mapping. *arXiv preprint arXiv:2302.07241*, 2023.
- Jiang, Y., Gupta, A., Zhang, Z., Wang, G., Dou, Y., Chen, Y., Fei-Fei, L., Anandkumar, A., Zhu, Y., and Fan, L. Vima: General robot manipulation with multimodal prompts. *arXiv preprint arXiv:2210.03094*, 2(3):6, 2022.
- Ke, T.-W., Gkanatsios, N., and Fragkiadaki, K. 3d diffuser actor: Policy diffusion with 3d scene representations. *arXiv preprint arXiv:2402.10885*, 2024.
- Kerr, J., Kim, C. M., Goldberg, K., Kanazawa, A., and Tancik, M. Lorf: Language embedded radiance fields. In *Proceedings of the IEEE/CVF international conference on computer vision*, pp. 19729–19739, 2023.
- Khazatsky, A., Pertsch, K., Nair, S., Balakrishna, A., Dasari, S., Karamcheti, S., Nasiriany, S., Srirama, M. K., Chen, L. Y., Ellis, K., et al. Droid: A large-scale in-the-wild robot manipulation dataset. *arXiv preprint arXiv:2403.12945*, 2024.
- Kim, M. J., Pertsch, K., Karamcheti, S., Xiao, T., Balakrishna, A., Nair, S., Rafailov, R., Foster, E., Lam, G., Sankeketi, P., et al. Openvla: An open-source vision-language-action model. *arXiv preprint arXiv:2406.09246*, 2024.
- Li, P., Wu, Y., Xi, Z., Li, W., Huang, Y., Zhang, Z., Chen, Y., Wang, J., Zhu, S.-C., Liu, T., et al. Controlvla: Few-shot object-centric adaptation for pre-trained vision-language-action models. *arXiv preprint arXiv:2506.16211*, 2025a.
- Li, Y., Deng, Y., Zhang, J., Jang, J., Memmel, M., Yu, R., Garrett, C. R., Ramos, F., Fox, D., Li, A., et al. Hamster: Hierarchical action models for open-world robot manipulation. *arXiv preprint arXiv:2502.05485*, 2025b.
- Liu, F., Fang, K., Abbeel, P., and Levine, S. Moka: Open-world robotic manipulation through mark-based visual prompting. *arXiv preprint arXiv:2403.03174*, 2024.
- Liu, H., Li, C., Wu, Q., and Lee, Y. J. Visual instruction tuning. *Advances in neural information processing systems*, 36:34892–34916, 2023.
- Liu, W., Du, Y., Hermans, T., Chernova, S., and Paxton, C. Structdiffusion: Language-guided creation of physically-valid structures using unseen objects. *arXiv preprint arXiv:2211.04604*, 2022.
- Lu, Y., Fan, Y., Deng, B., Liu, F., Li, Y., and Wang, S. VI-grasp: A 6-dof interactive grasp policy for language-oriented objects in cluttered indoor scenes. In *2023 IEEE/RSJ International Conference on Intelligent Robots and Systems (IROS)*, pp. 976–983. IEEE, 2023.
- Mirjalili, R., Jülg, T., Walter, F., and Burgard, W. Augmented reality for robots (arro): Pointing visuomotor policies towards visual robustness. *arXiv preprint arXiv:2505.08627*, 2025.
- Myers, A., Teo, C. L., Fermüller, C., and Aloimonos, Y. Affordance detection of tool parts from geometric features. In *2015 IEEE international conference on robotics and automation (ICRA)*, pp. 1374–1381. IEEE, 2015.
- Nair, S., Rajeswaran, A., Kumar, V., Finn, C., and Gupta, A. R3m: A universal visual representation for robot manipulation. *arXiv preprint arXiv:2203.12601*, 2022.
- OpenAI. Introducing gpt-5.2. <https://openai.com/index/introducing-gpt-5-2/>, 2025. Accessed: 2026-01-29.
- Parisi, S., Rajeswaran, A., Purushwalkam, S., and Gupta, A. The unsurprising effectiveness of pre-trained vision models for control. In *international conference on machine learning*, pp. 17359–17371. PMLR, 2022.
- Peng, S., Genova, K., Jiang, C., Tagliasacchi, A., Pollefeys, M., Funkhouser, T., et al. Openscene: 3d scene understanding with open vocabularies. In *Proceedings of the IEEE/CVF conference on computer vision and pattern recognition*, pp. 815–824, 2023.

- Radford, A., Kim, J. W., Hallacy, C., Ramesh, A., Goh, G., Agarwal, S., Sastry, G., Askell, A., Mishkin, P., Clark, J., et al. Learning transferable visual models from natural language supervision. In *International conference on machine learning*, pp. 8748–8763. PmLR, 2021.
- Ray, A., Duan, J., Tan, R., Bashkirova, D., Hendrix, R., Ehsani, K., Kembhavi, A., Plummer, B. A., Krishna, R., Zeng, K.-H., et al. Sat: Spatial aptitude training for multimodal language models. *arXiv e-prints*, pp. arXiv:2412, 2024.
- Reed, S., Zolna, K., Parisotto, E., Colmenarejo, S. G., Novikov, A., Barth-Maron, G., Gimenez, M., Sulsky, Y., Kay, J., Springenberg, J. T., et al. A generalist agent. *arXiv preprint arXiv:2205.06175*, 2022.
- Ren, T., Liu, S., Zeng, A., Lin, J., Li, K., Cao, H., Chen, J., Huang, X., Chen, Y., Yan, F., et al. Grounded sam: Assembling open-world models for diverse visual tasks. *arXiv preprint arXiv:2401.14159*, 2024.
- Shi, J., Qian, J., Ma, Y. J., and Jayaraman, D. Plug-and-play object-centric representations from “what” and “where” foundation models. In *ICRA*, 2024.
- Shridhar, M., Manuelli, L., and Fox, D. Cliport: What and where pathways for robotic manipulation. In *Conference on robot learning*, pp. 894–906. PMLR, 2022.
- Tao, S., Xiang, F., Shukla, A., Qin, Y., Hinrichsen, X., Yuan, X., Bao, C., Lin, X., Liu, Y., Chan, T.-k., et al. Maniskill3: Gpu parallelized robotics simulation and rendering for generalizable embodied ai. *arXiv preprint arXiv:2410.00425*, 2024.
- Team, B. R., Cao, M., Tan, H., Ji, Y., Chen, X., Lin, M., Li, Z., Cao, Z., Wang, P., Zhou, E., et al. Robobrain 2.0 technical report. *arXiv preprint arXiv:2507.02029*, 2025.
- Tong, P., Brown, E., Wu, P., Woo, S., IYER, A. J. V., Akula, S. C., Yang, S., Yang, J., Middepogu, M., Wang, Z., et al. Cambrian-1: A fully open, vision-centric exploration of multimodal llms. *Advances in Neural Information Processing Systems*, 37:87310–87356, 2024.
- Walke, H. R., Black, K., Zhao, T. Z., Vuong, Q., Zheng, C., Hansen-Estruch, P., He, A. W., Myers, V., Kim, M. J., Du, M., et al. Bridgedata v2: A dataset for robot learning at scale. In *Conference on Robot Learning*, pp. 1723–1736. PMLR, 2023.
- Wang, W., Ren, Y., Luo, H., Li, T., Yan, C., Chen, Z., Wang, W., Li, Q., Lu, L., Zhu, X., et al. The all-seeing project v2: Towards general relation comprehension of the open world. In *European Conference on Computer Vision*, pp. 471–490, 2024.
- Yang, A., Li, A., Yang, B., Zhang, B., Hui, B., Zheng, B., Yu, B., Gao, C., Huang, C., Lv, C., et al. Qwen3 technical report. *arXiv preprint arXiv:2505.09388*, 2025.
- Yuan, C., Joshi, S., Zhu, S., Su, H., Zhao, H., and Gao, Y. Roboengine: Plug-and-play robot data augmentation with semantic robot segmentation and background generation. *arXiv preprint arXiv:2503.18738*, 2025a.
- Yuan, W., Duan, J., Blukis, V., Pumacay, W., Krishna, R., Murali, A., Mousavian, A., and Fox, D. Robopoint: A vision-language model for spatial affordance prediction for robotics. *arXiv preprint arXiv:2406.10721*, 2024.
- Yuan, Y., Cui, H., Chen, Y., Dong, Z., Ni, F., Kou, L., Liu, J., Li, P., Zheng, Y., and Hao, J. From seeing to doing: Bridging reasoning and decision for robotic manipulation. *arXiv preprint arXiv:2505.08548*, 2025b.
- Yuan, Y., Cui, H., Huang, Y., Chen, Y., Ni, F., Dong, Z., Li, P., Zheng, Y., and Hao, J. Embodied-r1: Reinforced embodied reasoning for general robotic manipulation. *arXiv preprint arXiv:2508.13998*, 2025c.
- Yuan, Y., Cui, H., Huang, Y., Chen, Y., Ni, F., Dong, Z., Li, P., Zheng, Y., and Hao, J. Embodied-r1: Reinforced embodied reasoning for general robotic manipulation. *arXiv preprint arXiv:2508.13998*, 2025d.
- Zhang, J., Memmel, M., Kim, K., Fox, D., Thomason, J., Ramos, F., Bıyık, E., Gupta, A., and Li, A. Peek: Guiding and minimal image representations for zero-shot generalization of robot manipulation policies. *arXiv preprint arXiv:2509.18282*, 2025.
- Zhao, Q., Lu, Y., Kim, M. J., Fu, Z., Zhang, Z., Wu, Y., Li, Z., Ma, Q., Han, S., Finn, C., et al. Cot-vla: Visual chain-of-thought reasoning for vision-language-action models. In *Proceedings of the Computer Vision and Pattern Recognition Conference*, pp. 1702–1713, 2025.
- Zheng, R., Liang, Y., Huang, S., Gao, J., Daumé III, H., Kolobov, A., Huang, F., and Yang, J. Tracevla: Visual trace prompting enhances spatial-temporal awareness for generalist robotic policies. *arXiv preprint arXiv:2412.10345*, 2024.
- Zitkovich, B., Yu, T., Xu, S., Xu, P., Xiao, T., Xia, F., Wu, J., Wohlhart, P., Welker, S., Wahid, A., et al. Rt-2: Vision-language-action models transfer web knowledge to robotic control. In *Conference on Robot Learning*, pp. 2165–2183. PMLR, 2023.

---

**Appendix Table of Contents**

<b>A The Embodied Grasping Annotation Framework</b>	<b>13</b>
A.1 System Architecture and Multi-Modal Viewport Synchronization	13
A.2 Action Semantic Templating and Output Schema	14
<b>B Trajectory Extraction and Control Algorithms</b>	<b>14</b>
B.1 3D Trajectory Extraction and Processing Pipeline	14
B.2 Hierarchical Visual Masking for Long-Horizon Manipulation	15
<b>C Single-Arm Task Suite Definitions</b>	<b>16</b>
C.1 Data Collection Protocol and Environmental Diversity	16
C.2 Detailed Design of the 14 Single-Arm Tasks	16
<b>D Dataset and Experimental Setup</b>	<b>18</b>
D.1 PeractOneCam Benchmark Tasks	18
D.2 Dataset Statistics and Generalization Protocol	18
<b>E Qualitative Visualizations</b>	<b>18</b>
E.1 Pre-processing: SAM2 Segmentation	18
E.2 Evaluation: 2D Trajectory Generation (Ours vs GT)	19
<b>F Training Prompts and Data Formats</b>	<b>20</b>
F.1 Multimodal Prompt Templates	20
F.2 Unified Dataset JSON Representation	20
<b>G Real-World Experimental Setup</b>	<b>21</b>
G.1 Task Definitions	21
<b>H Implementation Details</b>	<b>22</b>
H.1 High-Level VLM Tuning (Qwen3-VL)	22
H.2 Low-Level Policy Training (3DDA and 3DFA)	22
<b>I Detailed Experimental Results and Metric Definitions</b>	<b>23</b>
I.1 2D Tasks: Visual Grounding and Manipulation	23
I.2 3D Tasks: Spatial Reasoning and Depth Estimation	24
I.3 4D Tasks: Long-Horizon Planning	24

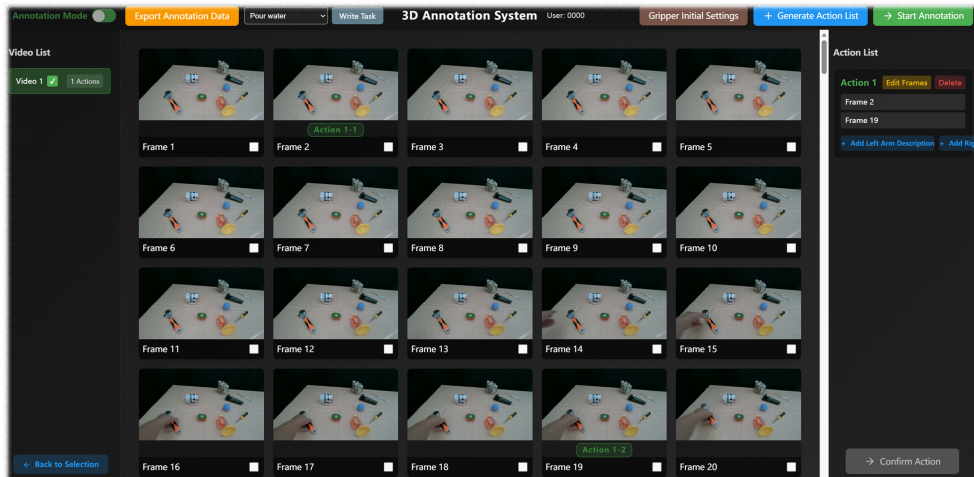
## A. The Embodied Grasping Annotation Framework

### A.1. System Architecture and Multi-Modal Viewport Synchronization

Our specialized annotation suite is engineered using the React-Three-Fiber framework. As illustrated in Figure 6, the workflow is divided into two operational stages to ensure precision:

1. **Video Selection (Top Panel):** Annotators perform temporal segmentation using a frame-grid interface to define the start and end indices of atomic actions. The "Action List" sidebar allows for the management of complex, multi-step task sequences.
2. **Data Labeling (Bottom Panel):** The core spatial annotation interface features a large **3D Point Cloud View** equipped with a 6-DoF gizmo for precise coordinate manipulation. Crucially, a **Synchronized 2D Preview** window (bottom-left) instantly renders the projection of 3D labels onto the RGB frame ( $P_{2D} = K[R|t]P_{3D}$ ), providing closed-loop visual verification to minimize depth-perception errors.

### Video Selection



### Data Labeling

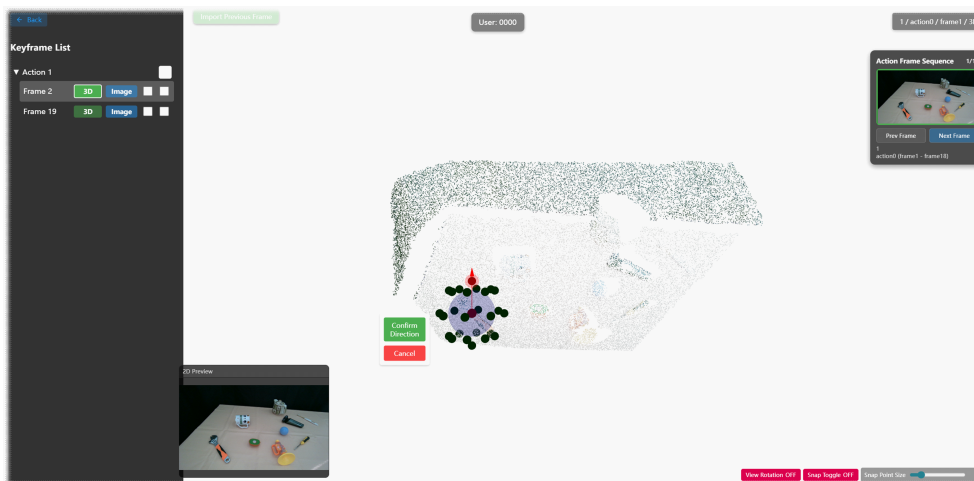


Figure 6. Overview of the Annotation Software Workflow. **Top:** The *Video Selection* interface for temporal segmentation, displaying frame sequences and action management lists. **Bottom:** The *Data Labeling* interface featuring a central 3D point cloud editor (with manipulation gizmo), strictly synchronized with a 2D RGB preview window (bottom-left) to ensure spatial-visual alignment.

- **Tier 00 (Annotation):** Operators define 6-DoF trajectory points, boolean gripper states ("0"=open, "1"=closed), and temporal boundaries.
- **Tier 01 (Audit):** A 100% manual review process where senior experts verify every annotated segment for spatial accuracy (< 5 mm deviation) and temporal alignment.
- **Tier 10 (Acceptance):** Automated statistical sampling. A batch is only committed to the database if it achieves a > 95% pass rate in random checks.
- **Tier 11 (Admin):** Global configuration of user permissions and data export pipelines (JSON/Parquet).

## A.2. Action Semantic Templating and Output Schema

We utilize a library of 18 structured action templates to convert manual labels into machine-readable language instructions. Algorithm 1 illustrates the primary data structure (info.json) generated by our framework.

---

### Algorithm 1 Raw Annotation Data Output Schema

---

```

1: {
2:   "task_description": "Pouring Water",
3:   "action_descriptions": [ {
4:     "frame_range": { "start_frame": "frame1", "end_frame": "frame8" },
5:     "left_description": {
6:       "action_description": "Pick up the coffee goblet",
7:       "coordinate_description": {
8:         "coordinate_0": {
9:           "text": "Pick up the coffee goblet",
10:          "image_coordinates": [417, 170],
11:          "cartesian_coordinates": [-0.031, -0.115, 0.674, 0.153, 0.013, 0.633]
12:        } }
13:      }
14:    } ],
15:   "parameter_data": { "camera_intrinsics": "[[427.17, ...]]" }
16: }

```

---

---

## B. Trajectory Extraction and Control Algorithms

### B.1. 3D Trajectory Extraction and Processing Pipeline

The transformation of raw visual observations into smooth robotic actions is formalized in Algorithm 2.

---

#### Algorithm 2 3D Trajectory Extraction and Processing Pipeline

---

- 1: **Input:** Video  $V$ , Depth  $D$ , Initial Point  $p_{init}$
  - 2: **Step 1 (Tracking):** Initialize SAM2 on  $V$  with  $p_{init}$ . Generate 2D track  $T_{2D}$ . Apply linear interpolation for minor occlusions.
  - 3: **Step 2 (Filtering):** Compute motion vector  $\vec{v}$ . Discard points  $p_t$  where projection distance to  $\vec{v}$  exceeds threshold  $\epsilon$  (Outlier Rejection).
  - 4: **Step 3 (Fusion):** Retrieve depth  $z \leftarrow D(u, v)$ . Unproject to 3D space:  $P_{3D} = K^{-1} \cdot [u, v, 1]^T \cdot z$ .
  - 5: **Step 4 (Smoothing):** Apply `WeightedPolyFit` (degree=2) to ensure kinematic feasibility.
  - 6: **Step 5 (Sampling):** Downsample to  $K = 8$  uniform keypoints for canonical representation  $\Omega$ .
- 

While the spatial tube effectively filters the workspace, certain interactions require even finer granularity. To ensure precision at the interaction interface, we implement an endpoint proximity constraint. If no object is detected within a 10cm radius of the trajectory’s terminal waypoint  $p_K$ , the system automatically identifies the nearest object within this search domain as a relevant entity. This heuristic guarantees that the policy maintains focus on the target object or the destination of the manipulation.

### B.2. Hierarchical Visual Masking for Long-Horizon Manipulation

To mitigate environmental distractions in multi-stage tasks, we employ Algorithm 3.

---

#### Algorithm 3 Hierarchical Visual Masking for Long-Horizon Focus

---

- 1: **Input:** Instruction List  $L$ , Stage  $k$
  - 2: **while** Task not finished **do**
  - 3:    $\tau_{ref} \leftarrow \text{GetReferenceTrajectory}(\text{Stage } k)$
  - 4:    $M_{all} \leftarrow \text{SAM2Segment}(I_{rgb}, L[k])$
  - 5:    $M_{focus} \leftarrow \{m \in M_{all} \mid \text{Intersect}(m, \tau_{ref})\}$
  - 6:    $\hat{I}_{rgb} \leftarrow \text{Inpaint}(I_{rgb}, \text{Mask} = M_{all} \setminus M_{focus})$
  - 7:   Execute Policy  $\pi(\hat{I}_{rgb})$  until stage completion criteria met.
  - 8:    $k \leftarrow k + 1$
  - 9: **end while**
-

## C. Single-Arm Task Suite Definitions

### C.1. Data Collection Protocol and Environmental Diversity

Our dataset covers diverse manipulation primitives **including fluid pouring, cloth folding, and multi-object assembly**. Using a fixed RGB-D sensor, we capture kinematically feasible human demonstrations where the hand exits the view between modular grasp-and-release cycles to ensure clean temporal segmentation.

To promote robust open-world generalization, we systematically vary lighting, background textures, and object attributes, and introduce random distractors during collection. The primary axes of variation include:

1. **Object Semantics:** Systematic variation of **color, material, and geometry** (e.g., stiffness of cables, opacity of bottles).
2. **Pose Randomization:** Objects are instantiated with random  $SE(2)$  poses on the desktop surface.
3. **Environmental Factors:** Integration of  $\geq 20$  desktop textures and randomized lighting conditions.

### C.2. Detailed Design of the 14 Single-Arm Tasks

This section details the operational design for the single-arm manipulation subset (approx. 800,000 frames).

#### Task 1: Pouring Water (40k Frames)

*Objective:* Transfer liquid from a source container to a target container.

*Core Variables:* Fluid interactions, container opacity, shape diversity (kettles, bottles, tea cups).

*Procedure:* Grasp source object, translate to target vicinity, rotate until liquid is transferred, and return to upright.

#### Task 2: Wiping Surfaces (40k Frames)

*Objective:* Clean a spill (liquid or powder) using a cleaning tool.

*Core Variables:* Stain types (colored liquids, coffee powder), tool types (sponges, rags).

*Procedure:* Retrieve tool, execute planar wiping motion (linear/circular) covering the stain area.

#### Task 3: Stacking Cups (80k Frames)

*Objective:* Stack 5 paper cups into a stable pyramid structure.

*Core Variables:* Cup deformation, texture variations ( $> 10$  styles), initial scattering.

*Procedure:* Precise pick-and-place with vertical alignment and gravity stability.

#### Task 4: Building Blocks (80k Frames)

*Objective:* Assemble blocks into specified shapes (numbers, animals, trees).

*Core Variables:* Block colors/shapes, target topology (requires  $\geq 5$  blocks).

*Procedure:* Sequentially pick blocks from random piles and place them to form connected 2D/3D structures.

#### Task 5: Pick and Place (Categorization) (110k Frames)

*Objective:* Sort objects into specific containers (boxes, drawers).

*Core Variables:* Object categories (toys, food, stationery), container types (bins, shelves).

*Procedure:* Identify object category, transport to matched container, and release safely.

#### Task 6: Scene Cleaning (25k Frames)

*Objective:* Clear desktop by moving trash items to a bin.

*Core Variables:* Trash types (crumpled paper, peel), bin location/type.

*Procedure:* Grasp irregular trash objects and release them above the disposal zone.

#### Task 7: Control Adjustment (40k Frames)

*Objective:* Operate mechanical controls such as valves, knobs, or buttons.

*Core Variables:* Mechanism types (rotary valves, push buttons, switches).

*Procedure:* Fine-grained manipulation: grasp handle and rotate (CW/CCW), or apply force to buttons.

#### Task 8: Target Placement (150k Frames)

*Objective:* Place objects in specific relative poses (e.g., "to the left of X", "upside down").

*Core Variables:* Relative semantics (left/right/in/on), 6-DoF orientation requirements.

*Procedure:* Pick object, re-orient gripper for target pose, and place according to spatial instruction.

**Task 9: Tower Stacking (50k Frames)**

*Objective:* Stack  $\geq 4$  objects (books, boxes) vertically without collapse.

*Core Variables:* Object friction, size ratios, center-of-mass estimation.

*Procedure:* Iteratively stack items, ensuring alignment of centers to maintain tower balance.

**Task 10: Push and Pull (40k Frames)**

*Objective:* Translate heavy or non-graspable objects across the surface.

*Core Variables:* Surface friction, obstacle placement, object mass.

*Procedure:* Apply non-prehensile force to slide objects to target zones, navigating around obstacles.

**Task 11: Point and Touch (100k Frames)**

*Objective:* Semantically reference object parts (e.g., "touch the blue handle").

*Core Variables:* Object parts, color, semantic regions.

*Procedure:* Move end-effector to close proximity of specific semantic regions without disrupting the object.

**Task 12: Material Cutting (50k Frames)**

*Objective:* Use a tool to cut deformable material (Play-doh) at a specific ratio.

*Core Variables:* Tools (knives), material consistency, cut ratios (1/2, 1/3).

*Procedure:* Grasp tool, align blade with semantic cut point, and execute downward shearing force.

**Task 13: Flexible Object Interaction (45k Frames)**

*Objective:* Manipulate deformable 1D objects (ropes, cables).

*Core Variables:* Stiffness, length, entanglement state.

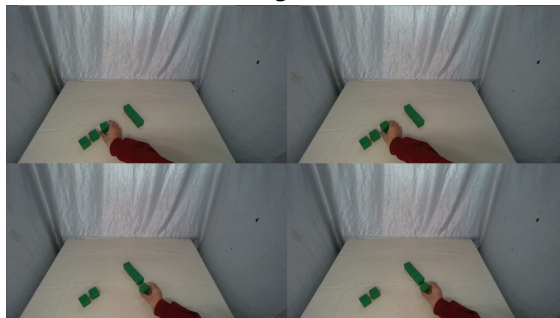
*Procedure:* Straighten, fold, or insert flexible linear objects into containers.

**Task 14: Spatial Position Swap (20k Frames)**

*Objective:* Swap locations of two objects.

*Procedure:* Multi-step planning: (1) Move Object A to buffer; (2) Move Object B to A's origin; (3) Move Object A to B's origin.

Building Blocks



Scene Cleaning

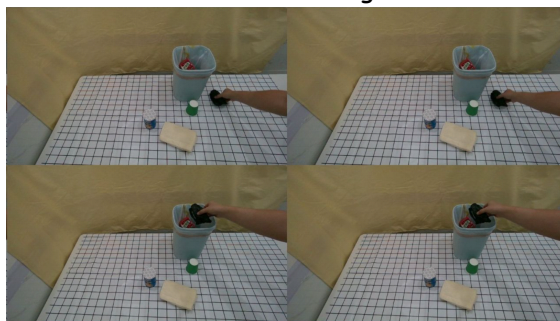


Figure 7. Qualitative Examples of Dataset Tasks. **Top:** 'Building Blocks' task demonstrating multi-object spatial arrangement. **Bottom:** 'Scene Cleaning' task showing interaction with irregular trash objects. Both examples highlight the diversity in background textures and lighting conditions.

## D. Dataset and Experimental Setup

### D.1. PeractOneCam Benchmark Tasks

We evaluate our method on a subset of the PeractOneCam dataset, focusing on four challenging long-horizon manipulation tasks:

**Close a jar:** There are two colored jars. The jar colors are sampled from a set of 20 colors. The agent needs to pick up the lid and screw it onto the jar with the specified color. The task involves six keyposes. **Screw a light bulb:** There are 2 light bulbs, 2 holders, and 1 lamp stand. The holder colors are sampled from a set of 20 colors. The agent needs to pick the correct light bulb and screw it into the matching colored holder. **Put groceries in the cupboard:** There are 9 YCB objects and a cupboard. The agent needs to grab the specified object and place it in the cupboard. The task involves 5 keyposes. **Push a button:** There are 3 buttons, whose colors are sampled from a set of 20 colors. The agent needs to push the colored buttons in the specified sequence. The task involves 3.8 keyposes on average.

### D.2. Dataset Statistics and Generalization Protocol

The dataset consists of expert trajectories collected in RLBench, with **100 episodes per task** for training. To assess generalization capabilities, we adopt a **Seen/Unseen** split protocol (Table 4) based on visual and semantic variations.

**Task Configurations and Generalization Rules.** For *Close Jar* and *Light Bulb In*, 5 of 20 color variations are held out to test zero-shot visual generalization. In *Put Groceries*, 2 of 9 object instances (e.g., Crackers, Soup) are excluded to evaluate semantic category transfer. For *Push Buttons*, we re-organize the original 50 variations—which involve sequential presses (1–3 times)—by decomposing them into single-press episodes. Specifically, trajectories are segmented every two keyposes, resulting in 78 variations across diverse button colors. This ensures each episode consists of exactly two keyposes, maximizing the model’s ability for precise language-to-color grounding.

Table 4. Dataset Statistics and Variation Splits. *Seen* indicates variations used for training (100 episodes/task); *Unseen* indicates variations held out for generalization testing.

Task Name	Total Vars	Seen	Unseen	Excluded Examples (Unseen)
Close Jar	20	15	5	Specific Colors (e.g., Azure, Violet)
Light Bulb In	20	15	5	Specific Colors (e.g., Black, White)
Put Groceries	9	7	2	Novel Objects (e.g., Crackers, Soup)
Push Buttons	78	78	0	None (Fine-grained Color Training)

## E. Qualitative Visualizations

This section provides qualitative examples of our pipeline’s intermediate processing (segmentation) and final model output (trajectory generation).

### E.1. Pre-processing: SAM2 Segmentation

We visualize the intermediate segmentation masks produced by SAM2 on three tasks. The robust mask generation is a critical precursor for accurate 3D lifting.

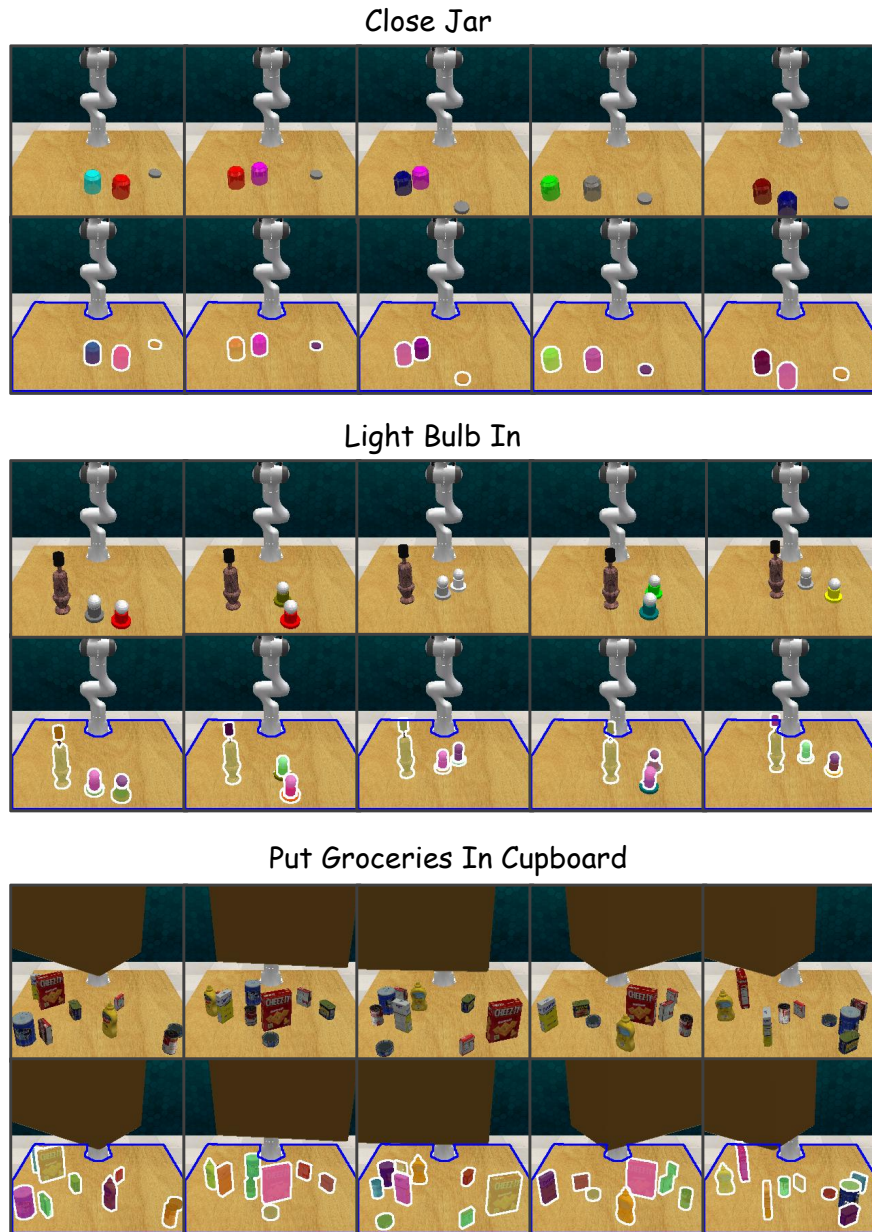


Figure 8. Qualitative Visualization of SAM2 Segmentation. **Top:** ‘Close Jar’ task, showing precise masks for colored jars and loose lids. **Middle:** ‘Light Bulb In’ task, isolating distinct components. **Bottom:** ‘Put Groceries In Cupboard’ task, demonstrating robust segmentation in clutter.

## E.2. Evaluation: 2D Trajectory Generation (Ours vs GT)

Figure 9 compares the 2D trajectories generated by our model against the ground truth (GT) human demonstrations.

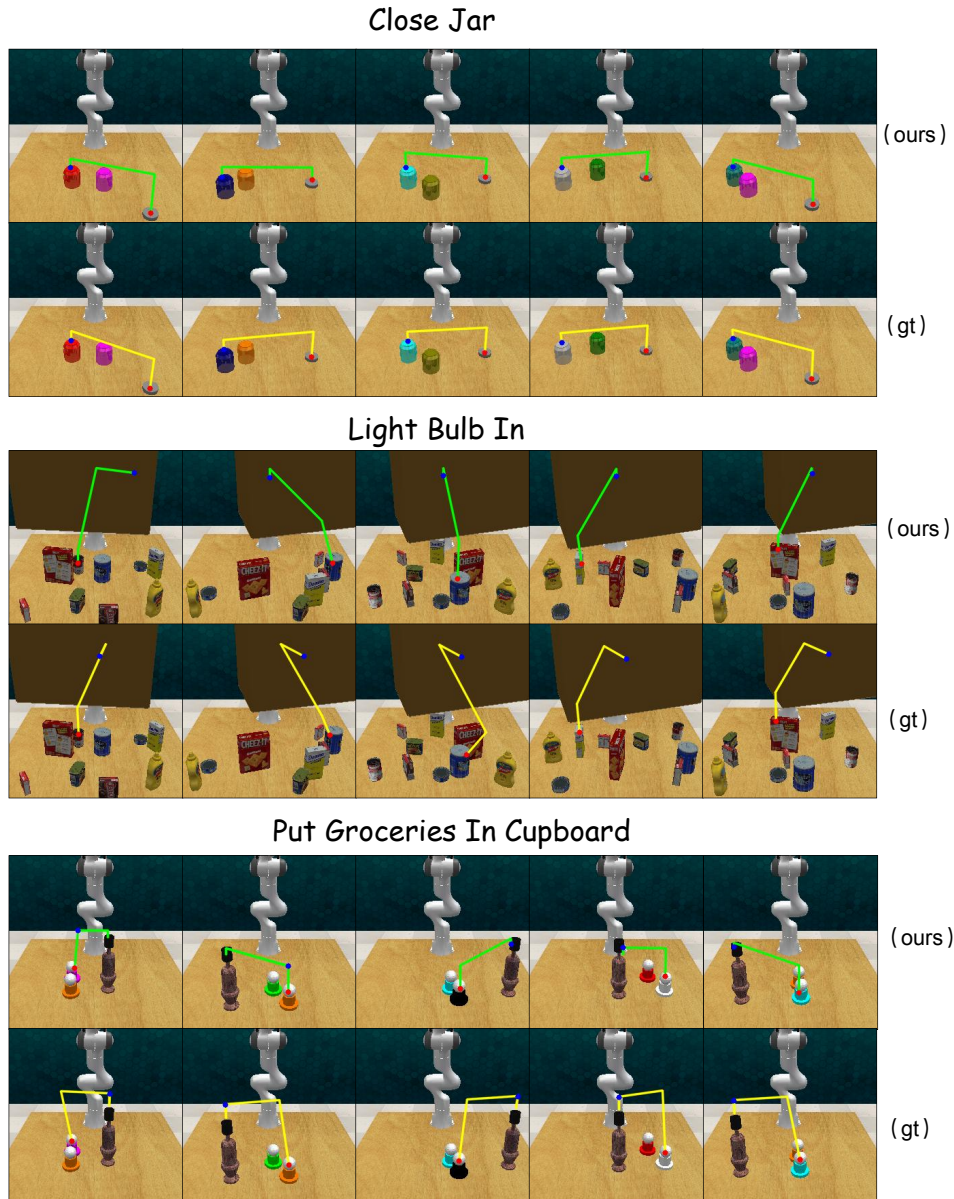


Figure 9. Qualitative Comparison of Trajectory Generation. We visualize the 2D trajectories generated by our model (top row) versus ground truth human demonstrations (bottom row) across three tasks: Close Jar (Left), Light Bulb In (Middle), and Put Groceries In Cupboard (Right). The model successfully captures the critical keypoints and temporal geometry of the manipulation paths.

## F. Training Prompts and Data Formats

### F.1. Multimodal Prompt Templates

We categorize training prompts into spatial, temporal, and reasoning tasks:

- **Trajectory:** "Instruction: '<task>'. Provide a sequence of exactly 8 points denoting the trajectory."
- **2D Grounding:** "Pinpoint a 2D point within <object>normalized to [0-1000]."

## F.2. Unified Dataset JSON Representation

Table 5 shows the data structure used for fine-tuning.

Table 5. Unified Dataset JSON Format

```
{
  "messages": [
    { "role": "user", "content": "<image>Task: 'Wipe table'." },
    { "role": "assistant", "content": "<bbox>...<bbox>" }
  ],
  "images": ["data/0001/rgb/frame_001.jpg"],
  "objects": {
    "traj_2d": [[500, 499], [516, 488], [534, 479], [552, 472],
    [571, 466], [590, 462], [611, 460], [631, 459]]
  }
}
```

## G. Experimental Setup for Real World

**Robot Setup.** We conduct real-world experiments using a Franka Emika Panda robot arm, a 7-DoF manipulator equipped with a standard parallel-jaw gripper. To perceive the environment, we utilize a third-person front-view camera positioned on a tripod facing the workspace. This camera provides a global perspective of the tabletop and the manipulation targets. The robot is controlled via a workstation running Linux, communicating with the robot controller in real-time.

### Task Definitions

#### (a) pick\_place

**Task Description:** The robot must grasp a target object (colored block or other item) and place it securely into a plate.

**Success Metric:** The task is successful if the object rests stably inside the boundaries of the plate after release.

**Objects:** Target object (variable color/type), one plate.

**Language Instructions:** *Put the <color>block in the plate. (or Put the <object> in the plate.)*

**Variation Number:** 4

#### (b) stack\_cube

**Task Description:** The robot must pick up a specific colored block and stack it on top of another block.

**Success Metric:** The task is successful if the top block is stably aligned on the bottom block without toppling for 5 seconds.

**Objects:** Two colored blocks.

**Language Instructions:** *Stack the <color1>block on the <color2>block.*

**Variation Number:** 6

Table 6. Properties of atomic tasks in real-world experiments.

Task name	Language Template	Variations	Variation Type
pick_place	“Put the <color> block in the plate.” (or “Put the <object> in the plate.”)	4	Color, Object Type
stack_cube	“Stack the <color1> block on the <color2> block.”	6	Color Pair

## H. Implementation Details

### H.1. High-Level VLM Tuning (Qwen3-VL)

We utilize the Qwen/Qwen3-VL-4B-Instruct model as our high-level planner. Table 7 details the hyperparameters used for the Supervised Fine-Tuning (SFT) process, where we employ LoRA targeting all linear modules to ensure efficient adaptation while preserving the pre-trained capabilities.

### H.2. Low-Level Policy Training (3DDA and 3DFA)

We provide the detailed hyperparameters used for training our 3DDA and 3DFA models in Table 8. The 3DDA model utilizes a DDPM-based diffusion process with 100 timesteps, employing a CLIP backbone for robust visual feature extraction. In contrast, the 3DFA model adopts a Rectified Flow formulation with only 5 denoising timesteps to enable rapid inference while maintaining generation quality. Both models are trained for 300,000 iterations with a batch size of 64.

Table 7. Hyperparameters for Qwen3-VL SFT Training

Parameter	Value
<i>Training Optimization</i>	
Model	Qwen/Qwen3-VL-4B-Instruct
Training Type	LoRA
Batch Size (Per Device)	6
Gradient Accumulation Steps	2
Total Batch Size	$6 \times 2 \times 8 = 96$
Learning Rate	$1 \times 10^{-4}$
Weight Decay	Default (not specified)
Warmup Ratio	0.05
Num Epochs	1
Mixed Precision	bfloat16
DeepSpeed Strategy	ZeRO-2
<i>LoRA Configuration</i>	
LoRA Rank	64
LoRA Alpha	128
Target Modules	all-linear
Freeze ViT	True
Freeze Aligner	True
<i>Multimodal &amp; Sequence</i>	
Max Length	4096
Max Image Tokens	1024
Max Video Tokens	128
Max Video Frames (FPS)	16
Packing	True
Padding Free	True
Attention Implementation	Flash Attention
<i>Dataset &amp; System</i>	
Validation Split Ratio	0.01
Num Workers (Dataloader)	4
Dataset Processes	8
Checkpoint Limit	10
Evaluation/Save Steps	50

Table 8. Hyperparameters for Peract Training and Evaluation

Parameter	Value
<i>Training Optimization</i>	
Batch Size	64
Learning Rate	$1 \times 10^{-4}$
Backbone Learning Rate	$1 \times 10^{-6}$
Weight Decay	$1 \times 10^{-10}$
LR Scheduler	Constant
Training Iterations	300,000
<i>Model Architecture</i>	
Model Type	Denoise3D
Backbone	CLIP
Embedding Dimension	120
Attention Heads	8
Vis-Instr Attention Layers	2
Shared Attention Layers	4
History Length	3 frames
FPS Subsampling Factor	4
Rotation Format	Quaternion (xyzw)
<i>Diffusion / Denoising</i>	
Denoise Model for 3DDA	DDPM
Denoise Timesteps for 3DDA	100
Denoise Model for 3DFA	RectifiedFlow
Denoise Timesteps for 3DFA	5
Prediction Length	1 (Keypose Only)
<i>Evaluation Environment</i>	
Image Size	$256 \times 256$
Max Steps	25
Max Tries (Motion Planner)	1
Dataset	PeractOneCam (front)
Seed	0 - 2

## I. Detailed Experimental Results and Metric Definitions

In this appendix, we provide a comprehensive breakdown of the experimental results across 2D, 3D, and 4D benchmarks. We evaluate models on both standard public datasets and our collected **ST-Human** suite. The detailed metric definitions are as follows:

### I.1. 2D Tasks: Visual Grounding and Manipulation

The 2D tasks evaluate the model’s capability in precise visual pointing and fine-grained trajectory generation. The quantitative results are shown in Table 9.

- **Hit Rate** ( $\uparrow$ ): For standard pointing tasks, we calculate the hit rate based on ground truth annotations.
  - **Point-in-Box**: Used for *RoboRefit* and *VABench-Point* (Yuan et al., 2025b). A prediction is correct if it falls within the ground-truth bounding box.
  - **Point-in-Mask**: Used for *Where2Place* and *Part-Afford* (Myers et al., 2015) A prediction is correct if it falls within the target segmentation mask.
- **ST-Human-Pointing Metrics**: For our self-collected pointing dataset, we evaluate both the **Mean Euclidean Distance (MED)** ( $\downarrow$ ) and the **Success Rate (SR)** ( $\uparrow$ ). Success is defined as the proportion of samples where the prediction error is below a pre-defined pixel threshold. (Table 9 reports SR).

- **Trajectory Metrics** ( $\downarrow$ ): For trajectory generation tasks (*VABench-Vision*, *RLBench*, *ST-Human-Trajectory*), we report the **Root Mean Square Error (RMSE)** and **Mean Absolute Error (MAE)**. Lower values indicate trajectories closer to human demonstrations.

Table 9. **Evaluation on 2D Tasks.** Metric types include: **Box-Hit** (RoboRefit, VAB-P), **Mask-Hit** (W2Pl, Afford), and **Success Rate** (ST-Human-Point). For trajectory tasks, we report RMSE ( $\downarrow$ ).

Method	RoboRefit	Where2Place	VABench-P	Part-Afford	ST-Human-Pointing	VABench-V $\downarrow$	RLBench $\downarrow$	ST-Human-Traj $\downarrow$
<i>Closed-source models</i>								
GPT-5.2	16.65%	43.00%	60.33%	23.50%	20.50%	174.00	66.34	130.08
Gemini-3-flash	57.75%	<b>87.00%</b>	61.00%	<b>86.00%</b>	75.50%	122.00	72.82	42.36
<i>Open-source models</i>								
Embodied-R1-3B	85.05%	66.83%	<b>73.50%</b>	44.74%	61.00%	72.10	65.89	78.85
PEEK-3B	10.05%	14.00%	17.33%	8.95%	3.00%	188.89	81.59	193.04
Robobrain2.0-3B	50.61%	61.00%	26.88%	28.35%	65.50%	153.86	72.98	71.76
Qwen3v1-4B	83.63%	65.00%	23.17%	28.40%	27.50%	191.90	95.80	348.50
<b>ST-VLA (Ours)</b>	<b>88.15%</b>	73.00%	59.67%	49.40%	<b>96.50%</b>	<b>70.65</b>	<b>41.27</b>	<b>16.91</b>

## I.2. 3D Tasks: Spatial Reasoning and Depth Estimation

Table 10 presents the results for 3D understanding.

- **QA Accuracy** ( $\uparrow$ ): For spatial relationship tasks (*CVBench*, *CRPE*, *SAT*, *Blink*, *ST-Human-Spatial*), the model is evaluated in a multiple-choice format. We report the standard accuracy. *Notably, ST-VLA exhibits a performance gap on CRPE compared to CVBench and SAT. We attribute this to CRPE’s emphasis on fine-grained geometric perception (e.g., precise depth ordering and occlusion), whereas datasets like CVBench focus more on high-level semantic spatial relationships, which align better with the action-oriented nature of our model.*
- **Depth Metrics:** For the *ST-Human-Depth* task:
  - **Ratio Accuracy** ( $\uparrow$ ): The proportion of samples where the predicted depth error is within 20% of the ground truth value.
  - **MAD** ( $\downarrow$ ): The Mean Absolute Deviation in centimeters.

Table 10. **Evaluation on 3D Tasks.** Spatial tasks use multiple-choice accuracy. Depth estimation reports Ratio Accuracy (threshold 20%) and MAD.

Method	CVBench	CRPE	SAT		Blink	ST-Human-Spatial	ST-Human-Depth	
			Val	Test			Ratio Acc $\uparrow$	MAD(cm) $\downarrow$
<i>Closed-source models</i>								
GPT-5.2	79.62%	78.89%	66.56%	66.00%	49.08%	68.00%	4.00%	12.22
Gemini-3-flash	83.94%	<b>80.21%</b>	62.63%	64.67%	56.23%	84.00%	6.00%	13.82
<i>Open-source models</i>								
Embodied-R1-3B	81.69%	74.78%	74.66%	70.00%	<b>62.26%</b>	56.00%	2.70%	54.00
PEEK-3B	55.49%	64.55%	50.76%	52.67%	40.35%	50.00%	0.00%	10.00
Robobrain2.0-3B	81.22%	73.03%	59.64%	69.33%	51.24%	48.00%	8.89%	10.31
Qwen3v1-4B	79.21%	77.89%	65.75%	68.67%	62.13%	62.00%	9.33%	14.07
<b>ST-VLA (Ours)</b>	<b>84.52%</b>	73.67%	<b>93.48%</b>	<b>75.33%</b>	50.00%	<b>98.00%</b>	<b>46.67%</b>	<b>1.82</b>

## I.3. 4D Tasks: Long-horizon Planning

Table 11 details the evaluation on the *ST-Human-Planning* dataset.

- **Instruction Prediction** ( $\uparrow$ ): For predicting the *Next* and *Previous* instructions, we compute the **BERTScore** to measure semantic similarity with ground-truth texts.
- **Task Progress Estimation:**
  - **Step Acc** ( $\uparrow$ ): The proportion of samples where the predicted step index exactly matches the ground truth.
  - **Step MAE** ( $\downarrow$ ): The average absolute deviation of the predicted step index.
  - **Status Acc** ( $\uparrow$ ): A binary classification accuracy measuring if the model correctly identifies whether the task has finished.
- **Next-Step Trajectory** ( $\downarrow$ ): We evaluate the planned future trajectory using **RMSE** and **MAE**.

Table 11. **Evaluation on 4D Tasks (ST-Human-Planning)**. Evaluating instruction generation (BERTScore), progress estimation (Step/Status metrics), and future planning error.

Method	Next Act	Prev Act	Progress Estimation			Plan Error $\downarrow$	
	BERT $\uparrow$	BERT $\uparrow$	Step Acc $\uparrow$	Step MAE $\downarrow$	Status Acc $\uparrow$	RMSE	MAE
<i>Closed-source models</i>							
GPT-5.2	0.89	0.88	12.00%	4.62	88.0%	199.35	186.77
Gemini-3-flash	0.83	0.82	16.00%	4.10	84.0%	283.47	245.50
<i>Open-source models</i>							
Embodied-R1-3B	0.79	0.78	14.00%	4.48	78.0%	129.94	76.86
PEEK-3B	0.77	0.80	14.00%	4.90	88.0%	178.29	109.78
Robobrain2.0-3B	0.88	0.88	18.00%	4.50	88.0%	256.94	253.11
Qwen3v1-4B	0.77	0.70	14.00%	4.78	88.0%	448.75	394.96
<b>ST-VLA (Ours)</b>	<b>0.97</b>	<b>0.98</b>	<b>60.00%</b>	<b>0.70</b>	<b>92.0%</b>	<b>43.66</b>	<b>24.13</b>